

Article

Hierarchical Model Updating Method for Vector Electric-Propulsion Satellites

Xueqian Wu  and Yunfeng Dong * 

School of Astronautics, Beihang University, Beijing 100191, China; wuxueqian@buaa.edu.cn

* Correspondence: sinosat@buaa.edu.cn; Tel.: +86-133-0102-0700

Abstract: Electric propulsion is of great significance to the development of high-efficiency and long-life satellites, and digital twins have gradually become a powerful tool for satellite engineering. Being affected by uncertainty factors such as the complexity and variability of the space environment and the satellite system, the digital twin model cannot accurately reflect the real physical properties. Therefore, it is crucial to update the satellite model to improve prediction accuracy. However, the complex structure and multi-physics process coupling of vector electric-propulsion satellites bring great challenges to model updating. According to the characteristics of the vector electric-propulsion satellite, this paper establishes mathematical models of the whole satellite. Additionally, a hierarchical model updating method is proposed and applied to the model updating case of a satellite with multiple subsystems. The simulation results show that the method is suitable for the model updating of the vector electric-propulsion satellite. Through multiple iterations of closed-loop cycles, the residual errors between the simulation values and the telemetry values can be decreased, and the errors between the estimated values and the true values of state variables can also be decreased by an order of magnitude.

Keywords: vector electric-propulsion satellite; digital twin; uncertainty quantification; hierarchical model updating



Citation: Wu, X.; Dong, Y.
Hierarchical Model Updating
Method for Vector
Electric-Propulsion Satellites. *Appl.
Sci.* **2023**, *13*, 4980. <https://doi.org/10.3390/app13084980>

Academic Editors: Mathieu
Balesdent, Loïc Brevault and
Jérôme Morio

Received: 22 March 2023

Revised: 10 April 2023

Accepted: 12 April 2023

Published: 15 April 2023



Copyright: © 2023 by the authors.
Licensee MDPI, Basel, Switzerland.
This article is an open access article
distributed under the terms and
conditions of the Creative Commons
Attribution (CC BY) license (<https://creativecommons.org/licenses/by/4.0/>).

1. Introduction

In contrast with traditional chemical propulsion, electric propulsion has the characteristics of low thrust force and high specific impulse [1], which are conducive to reducing fuel consumption [2] and prolonging the life of satellites. Therefore, it meets the requirements for geostationary Earth orbit (GEO) satellites, low Earth orbit (LEO) satellites, small satellites, and deep space probes to work on orbit in the long run [3]. It has also become an important development direction for new high-performance and long-life spacecraft.

In many countries, the manufacturing industry has shown the development trend of digitalization and intelligence [4]. As a technology that can realize the interaction and integration of the physical world and the digital world [5], the digital twin has attracted widespread attention. In 2010, the National Aeronautics and Space Administration (NASA) proposed to apply digital twins to flight training, accompanying flight, health monitoring, and parameter optimization [6]. By establishing a digital twin model of a satellite to perform optimization design and feedback control of real satellites, it is advantageous to reduce the cost and risk of decision-making.

Since the simulation model is different from the real physical entity and is affected by uncertainties, it is unable to fully reflect the characteristics of the real system and reduces the prediction accuracy. There are two categories of uncertainty sources in a digital twin, which are aleatory uncertainty and epistemic uncertainty [7]. Aleatory uncertainty refers to the intrinsic randomness of a system, which is inevitable and irreducible. For example, a thruster may have uncertainties such as the manufacturing tolerance of parts, installation error, thermal deformation of structural parts, and nonaxisymmetric installation

of cathodes [8], and these errors could cause the thruster to deviate from the nominal states. Epistemic uncertainty refers to uncertainty caused by limited data, lack of knowledge, or model simplifications and assumptions. It can be decreased when more information or data is available [9]. For example, many studies simplified the thruster to an ideal force model while ignoring the details of the mechanical structures when performing thrust calibration. The more simplifications are made, the more difficult it is to establish an accurate and reliable model. Therefore, it is essential to identify, describe and evaluate the uncertainties quantitatively, known as uncertainty quantification (UQ). The study of UQ includes the expression of uncertainty, the propagation of uncertainty, the identification of model parameters, and so on [10]. In this research, it refers in particular to the model updating method for the vector thruster satellite, with using the measurement data to estimate the errors and correct the simulation model so that the error between the model and the real satellite is minimized and the prediction level of the model could be improved.

According to the sources of uncertainty, model updating includes formula updating and parameter updating. Formula updating refers to the addition and modification of certain items in a mathematical formula. For instance, decoupling the coupled subsystems for separate calculations will result in some loss of accuracy. Parameter updating involves the use of measurement data to adjust model parameters without modifying the formula structure. This paper focuses on the latter.

Model parameter updating is essentially an optimization problem that can be solved using optimization algorithms, including traditional optimization methods and modern optimization methods. The former includes the least-squares method and filtering algorithm, while the latter includes particle swarm optimization (PSO) and genetic algorithms (GAs). All of them are widely used for parameter estimation. The modern optimization methods are time-consuming, whereas the traditional optimization method has a fast convergence speed, so the least-squares method is adopted in this paper.

Model updating for electric-propulsion satellites implies the multiparametric optimization of a large number of electric, magnetic, thermodynamic, and other processes [11]. From the perspective of the space dimension, the satellite is influenced by forces and moments from the environment. The satellite system itself can be divided into multiple subsystems, including the orbit and attitude control system; power system; thermal control system; propulsion system; and telemetry, telecommand, and control system. Each subsystem is further composed of many components. Additionally, there are coupling relationships between the environment and the subsystems, as well as the various components. As the functions and structures of satellites develop in a more complex and changeable direction, these coupling effects will become increasingly significant, and the physical properties and magnitudes of interactions will be more inconsistent, causing satellite model updating to be more challenging and resource-consuming. Since the amount of satellite parameters that need to be updated is large and the degree of coupling between different parameters is different, if all the parameters are updated simultaneously, there is a high probability that the solution will not converge. Thus, it is imperative to divide them into different hierarchies according to the degree of the sparseness of the interaction between parameters and then perform updating separately.

The hierarchical method means to divide the complex engineering system into subsystems; the subsystems are partitioned into components, the components into parts, and so on [12]. Oberkamp et al. proposed the use of a hierarchical model for model validation [13]. First, the characteristics of the corresponding model are confirmed by using the test data of the simple system, and then the whole system model is deduced recursively. The hierarchical idea reduces the complexity of solving the original problem, so it is also used in the model updating problem of multi-coupled complex systems [14]. Cheng et al. [15] divided parameters into key parameters and non-key parameters by sensitivity analysis. The key parameters were corrected first, then the non-key parameters, and finally, all parameters at the same time. This method had higher accuracy than directly correcting all parameters. He et al. [16] decomposed the landing buffer system into the recovery module and the

airbag system, and their finite element (FE) models were respectively established and updated. By considering the measurement uncertainty brought about by the high-temperature environment in the complex aeromechanical system, He et al. [17,18] and Chen et al. [19] identified the thermodynamic parameters and the mechanical structure parameters sequentially. Fei et al. [20] proposed a hierarchical model updating strategy for the FE model of complex structures, which decomposed the assembled structure into a series of substructures. These substructures were accurately modeled and updated. Xu et al. [21] proposed a two-stage hierarchical objective model updating pattern for cable force identification, and the method improved the accuracy and efficiency of FE model updating.

Since the thrust generated by electric propulsion is very small, in the order of millinewtons, the thrusters need to be turned on for a long time when performing an orbit mission. If the thrust direction does not exceed the center of mass of the satellite, an eccentric moment will be generated, and the angular momentum will be increased. In addition, since electric thrusters are also intended to perform attitude control tasks, most electric thrusters are equipped with vector adjustment mechanisms to change the thrust direction of the force. Each vector adjustment mechanism is composed of two rotating shafts so that the thrust direction can be changed in three dimensions, but this is also a reason why its motion parameters are coupled, and many parameters are involved. Due to the small thrust, it is difficult to complete high-precision thrust calibration on the ground. The commonly used thrust calibration methods include the parameter calibration method, wheel calibration method, and orbital calibration [22]. However, these methods simplify the thrust to a fixed vector without considering the influence of the error of the vector adjustment mechanism, nor do they consider the coupling effect between the other subsystems and the motion of the vector adjustment mechanism. Therefore, a challenge that needs to be tackled is how to create a hierarchical rule and model updating method to correct the parameters of a satellite with vector electric propulsion.

To address the problems mentioned above, this paper aims to develop a hierarchical model updating method for the vector electric-propulsion satellite. Firstly, in order to reflect the coupling effect between different parts, the whole satellite is decomposed into different subsystems and devices to establish mathematical models. The state variables that play a major role in affecting the telemetry variables are selected for updating. Then, a grouping rule is put forward in terms of the relationship of variables. State variables and telemetry variables are grouped and sorted according to the rule, and each group is updated by the least-squares method in sequence. When all groups are updated, the residuals of all groups are recalculated. Repeat this process several times until the mean squared error (MSE) converges to the specified range.

This paper is organized as follows. Section 2 presents the mathematical description of the model updating problem and establishes the simulation model of a vector electric-propulsion satellite. A hierarchical method for model updating is developed in Section 3. In Section 4, a simulation test case is investigated, and the results are discussed. Finally, Section 5 concludes this paper.

2. Problem Formulation

The satellite simulation model can be expressed as follows:

$$\begin{cases} \dot{x} = f(x, t) \\ y = g(x, t) \\ x(t_0) = x_0 \end{cases} \quad (1)$$

where $x \in \mathbb{R}^n$ is the vector of state variables, and $y \in \mathbb{R}^m$ is the vector of telemetry variables, which both change over time t ; $f(\cdot)$ are the state equations, and $g(\cdot)$ are measurement equations, the details of which are described in Sections 2.1 and 2.2; and x_0 is the initial value of state variables.

In the given period $t \in [t_0, t_f]$, the telemetry values are known as $y_j^{tele} = [y_j^{tele}(t_0), y_j^{tele}(t_1), \dots, y_j^{tele}(t_f)]$, $j = 1 \dots m$, and the model simulation values are known as $y_j^{sim} = [y_j^{sim}(t_0), y_j^{sim}(t_1), \dots, y_j^{sim}(t_f)]$, $j = 1 \dots m$. The telemetry value and simulation value at each moment are normalized by

$$\bar{y}_j^{tele}(t) = \frac{y_j^{tele}(t) - y_{j,\min}}{y_{j,\max} - y_{j,\min}} \quad (2)$$

$$\bar{y}_j^{sim}(t) = \frac{y_j^{sim}(t) - y_{j,\min}}{y_{j,\max} - y_{j,\min}} \quad (3)$$

where $y_{j,\min}$ and $y_{j,\max}$ are the minimum and maximum of y_j , respectively.

The goal of model updating is to minimize the MSE between the normalized simulation values and the normalized telemetry values by adjusting the initial value, x_0 ; that is,

$$\min_{x_0} mse_{total} = \frac{1}{2} \sum_{j=1}^m \sum_{i=0}^f [\bar{y}_j^{sim}(t_i) - \bar{y}_j^{tele}(t_i)]^2 \quad (4)$$

2.1. State Equations and State Variables

The orbit dynamics equations are

$$\begin{cases} \frac{dr}{dt} = v \\ \frac{dv}{dt} = \frac{1}{m}(F_E + F_A + F_C + F_P + F_T) \end{cases} \quad (5)$$

where $r = [r_x, r_y, r_z]^T$ is the position vector, $v = [v_x, v_y, v_z]^T$ is the velocity vector, m is the total mass, F_E is the Earth's gravitational force, F_A is the drag force, F_C is the perturbation force of the Sun and Moon, F_P is solar radiation pressure, and F_T is the force of thrusters.

The attitude dynamics equations are

$$\begin{cases} \frac{dQ}{dt} = \frac{1}{2}\Omega(\omega) \cdot Q \\ \frac{d\omega}{dt} = I^{-1}(M_{gg} + M_A + M_P + M_T + M_W - \omega \times H) \end{cases} \quad (6)$$

where $Q = [q_0, q_1, q_2, q_3]^T$ is the attitude quaternions of the body with respect to the inertial system, and $\omega = [\omega_x, \omega_y, \omega_z]^T$ is the angular velocity of the satellite's body frame with respect to the inertial frame. $\Omega(\omega)$ is a matrix with respect to ω :

$$\Omega(\omega) = \begin{bmatrix} 0 & \omega_z & -\omega_y & \omega_x \\ -\omega_z & 0 & \omega_x & \omega_y \\ \omega_y & -\omega_x & 0 & \omega_z \\ -\omega_x & -\omega_y & -\omega_z & 0 \end{bmatrix} \quad (7)$$

I is the inertia matrix, M_{gg} is the gravity gradient moment, M_A is the drag moment, M_P is the solar pressure moment, M_T is the thrusters moment, M_W is the wheels moment, and H is the angular momentum of the total satellite. The details of force and moment can be found in Reference [23].

Usually, the Euler angles are used to describe the attitude of the body relative to the orbit frame, which contain the roll angle φ , pitch angle θ , and yaw angle ψ . They can be calculated by Q , r , and v [23].

The rotation of solar wing can be described by

$$\begin{cases} \frac{d\theta_{wing}}{dt} = \dot{\theta}_{wing} \\ \frac{d\dot{\theta}_{wing}}{dt} = M_{wing} \end{cases} \quad (8)$$

where θ_{wing} and $\dot{\theta}_{wing}$ are the angle and angular speed of the solar wing related to the satellite body, respectively, and M_{wing} is the driving moment.

The output power of each solar array is

$$P_{Wing} = C_{shadow} S_0 A_{sa} \eta_w X_{Wing} \cos(\theta_{SW}) (\beta_P \Delta T_{wing} + 1) \quad (9)$$

where C_{shadow} is the shadow area sign, S_0 is the solar constant, A_{sa} is the area of the solar array, η_w is the photoelectric conversion efficiency, X_{Wing} is the other coefficient, θ_{SW} is the angle between the normal direction of the solar array and the direction of sunlight, β_P is the power temperature coefficient, and ΔT_{wing} is the difference between the working temperature of the solar array and the standard temperature; for a detailed calculation, see Reference [24].

When the output voltage of the solar wing U_{Wing} is known, the current can be calculated by

$$I_{Wing} = \frac{P_{wing}}{U_{wing}} \quad (10)$$

The total electric load power is

$$P_{Device} = \sum_{i=1}^{N_{PD}} P_{D_i} \quad (11)$$

where N_{PD} is the number of working devices, and P_{D_i} is the power of the i -th device.

When the difference between the output power and the load power is greater than the maximum charging power of the battery, the power consumed by the shunt regulator is

$$P_{Loss} = \begin{cases} P_{Wing} - P_{Device} - P_{MaxCharge}, & P_{Wing} - P_{Device} > P_{MaxCharge} \\ 0 & \text{else} \end{cases} \quad (12)$$

where $P_{MaxCharge}$ is the maximum charging power of the battery.

The battery charges when the battery is not full and the output power is greater than the load power, and it discharges when the battery quantity is greater than the minimum quantity and the electric power is smaller than the load power. The process is

$$P_{Battery} = \begin{cases} P_{Wing} - P_{Device} - P_{Loss}, & Q_{MinBattery} < Q_{Battery} < Q_{MaxBattery} \\ 0 & \text{else} \end{cases} \quad (13)$$

where $Q_{MinBattery}$ and $Q_{MaxBattery}$ are the minimum and maximum battery capacity, respectively.

The quantity change in the battery can be expressed as

$$\frac{dQ_{Battery}}{dt} = \begin{cases} k_{Charge} \cdot P_{Battery}, & P_{Battery} > 0 \\ k_{Discharge} \cdot P_{Battery}, & P_{Battery} < 0 \end{cases} \quad (14)$$

where $Q_{Battery}$ is the remaining quantity, k_{Charge} is the charging coefficient, and $k_{Discharge}$ is discharging coefficient.

The battery voltage

$$U_{Battery} = \begin{cases} U_{Charge}, & P_{Battery} > 0 \\ U_{Discharge}, & P_{Battery} < 0 \end{cases} \quad (15)$$

where U_{Charge} is the charge voltage, and $U_{Discharge}$ is the discharge voltage.

The battery current is

$$I_{Battery} = \frac{P_{Battery}}{U_{Battery}} \quad (16)$$

The mass of xenon in the xenon tank is

$$\frac{dm_{Xe}}{dt} = \dot{m}_{control} \quad (17)$$

where $\dot{m}_{control}$ is the mass rate controlled by the computer on board.

Each thruster is connected to two xenon tanks by a pipeline with different regulating valves. Only when the thruster receives the fire command and the pipeline between the xenon tank and the thruster is open, the thruster is working. The electric thrust force generated is

$$F_T = I_{sp} \cdot g \cdot \frac{dm_{Xe}}{dt} \quad (18)$$

where I_{sp} is the specific impulse, and g is the gravitational acceleration.

The gas state of the xenon satisfies the ideal gas equation of state. When the volume V_{Xe} is fixed, the pressure is

$$P_{Xe} = \frac{R_{gas} T_{Xe}}{M_{Xe} V_{Xe}} \cdot m_{Xe} \quad (19)$$

where M_{Xe} is the average molar mass of xenon, R_{gas} is the gas constant, and T_{Xe} is the temperature.

The temperature field model is calculated by finite element mesh division of the satellite model with Ansys, and each grid represents a node. The temperature of node i can be calculated by the heat balance equation:

$$\frac{dT_i}{dt} = \frac{q_S^i + q_E^i + q_{ER}^i + q_{Rad}^i + q_{Cond}^i + P_i - q_{OS}^i - q_{IS}^i}{m_i c_i} \quad (20)$$

where q_S^i is solar radiation received by node i , q_E^i is The heat from the Earth's infrared radiation, q_{ER}^i is the Earth's albedo heat, q_{Rad}^i is the thermal radiation from other thermal nodes to node i , q_{Cond}^i is heat conduction from other thermal nodes to node i , P_i is total thermal power of all components in the range of node i , q_{OS}^i is dissipate heat for the outer surface of node i , q_{IS}^i is heat dissipation for the inner surface of node i , m_i is mass of node i , and c_i is specific heat capacity. The details are in Reference [25].

The thermal control unit model includes a temperature sensor and a heater. The power of the heater is

$$P_{ht} = I_{ht}^2 R_{ht} = \frac{U_{ht}^2}{R_{ht}} \quad (21)$$

where I_{ht} , U_{ht} , R_{ht} are the current, voltage, and resistance of the heater, respectively.

For the sensors, the error is assumed to follow a normal distribution, and the error characteristic is described by the mean value μ_{sensor} and variance σ_{sensor} , which are constant:

$$\begin{cases} \frac{d\mu_{sensor}}{dt} = 0 \\ \frac{d\sigma_{sensor}}{dt} = 0 \end{cases} \quad (22)$$

We include the variables $\mu_{GPS,r}, \sigma_{GPS,r}$ when the Global Positioning System (GPS) measures r ; the variables $\mu_{GPS,v}, \sigma_{GPS,v}$ when the GPS measures v ; and the variables $\mu_{StarSensor}, \sigma_{StarSensor}$ when the star sensor measures attitude. As for the gyro, besides $\mu_{Gyro,\omega}, \sigma_{Gyro,\omega}$, there still exists the drift error $\varepsilon_{Gyro,\omega}$, which changes as

$$\frac{d\varepsilon_{Gyro,\omega}}{dt} = -\frac{\varepsilon_{Gyro,\omega}}{T} + \sigma_{Gyro,\omega} \quad (23)$$

The actuators include wheels, thrusters, and a rotating component of the solar wing. The output process noise is also represented by a normal distribution:

$$u_{output} = u_{expect} + N(\mu_{Actuator,u}, \sigma_{Actuator,u}) \quad (24)$$

where u_{expect} is the expected output command, u_{output} is actual output control, and $\mu_{Actuator,u}, \sigma_{Actuator,u}$ are the error mean and variance of the actuator output process, respectively. The sensor model and actuator model are described in Reference [23].

Four vector thrusters are installed on the backboard of the satellite, their installation positions and serial numbers are upper left T_{N1} , upper right T_{N2} , lower left T_{S1} , and lower right T_{S2} , respectively. Each thruster is connected to the satellite body by a vector adjustment mechanism, which is regarded as a structure of two links, each of which can rotate on its axis. The two-degree-of-freedom kinematic model can be described by eight parameters including connecting rod angle α_{i-1} , connecting rod length a_{i-1} , joint angle θ_i , and connecting rod offset d_i ($i = 1, 2$). The meaning of these parameters and the kinematic process are shown in Reference [26].

According to the model, the thrust direction is only related to θ_i , and the application point of thrust is related to all structural parameters. The thruster number is denoted by No ($No = N1, N2, S1, S2$); the structural error includes the length error $\delta\alpha_{i-1,No}$ and offset error $\delta d_{i,No}$. Three attitude angles $\varphi_{T_{No}}^{Install}, \theta_{T_{No}}^{Install}, \psi_{T_{No}}^{Install}$ are available for mounting attitude. Installation points are represented by position vectors $[X_{T_{No}}^{Install}, Y_{T_{No}}^{Install}, Z_{T_{No}}^{Install}]^T$. Every time it fires, the deflection error of the thrust direction at the outlet relative to the axis is represented by $\delta_{T_{No}}, \gamma_{T_{No}}$, and the output force action point error $\delta p_{T_{No}} = [\delta p_{x,T_{No}}, \delta p_{y,T_{No}}, \delta p_{z,T_{No}}]^T$. The above variables are constant values during the working period of each firing. Furthermore, the output force of the thruster $F_{T_{No}}$ is not a constant value but a variable that changes with time. In this paper, the parameters of the thruster T_{N1} are taken as the updating variables.

In summary, x consists of

$$x = [r_x, r_y, r_z, v_x, v_y, v_z, \varphi, \theta, \psi, \omega_x, \omega_y, \omega_z, \theta_{wing1}, \theta_{wing2}, \theta_{SW1}, \theta_{SW2}, \eta_w, P_{wing1}, P_{wing2}, U_{wing1}, U_{wing2}, I_{wing1}, I_{wing2}, Q_{Battery}, P_{Battery}, I_{Battery}, m_{Xe}, P_{Xe}, T_i, \mu_{GPS,r}, \sigma_{GPS,r}, \mu_{GPS,v}, \sigma_{GPS,v}, \mu_{Gyro,\omega}, \sigma_{Gyro,\omega}, \varepsilon_{Gyro,\omega}, \mu_{StarSensor}, \sigma_{StarSensor}, \varphi_{T_{N1}}^{Install}, \theta_{T_{N1}}^{Install}, \psi_{T_{N1}}^{Install}, X_{T_{N1}}^{Install}, Y_{T_{N1}}^{Install}, Z_{T_{N1}}^{Install}, \delta_{T_{N1}}, \gamma_{T_{N1}}, \delta p_{x,T_{N1}}, \delta p_{y,T_{N1}}, \delta p_{z,T_{N1}}, F_{T_{N1}}] \quad (25)$$

2.2. Measurement Equations and Telemetry Variables

The measurement equations for the GPS' measured position and velocity are

$$r_{GPS} = r + N(\mu_{GPS,r}, \sigma_{GPS,r}) \quad (26)$$

$$v_{GPS} = v + N(\mu_{GPS,v}, \sigma_{GPS,v}) \quad (27)$$

where $r_{GPS} = [r_{xGPS}, r_{yGPS}, r_{zGPS}]^T$ is the position measurement, and $v_{GPS} = [v_{xGPS}, v_{yGPS}, v_{zGPS}]^T$ is the velocity measurement.

The error transmission process of the star sensor is shown in Reference [23], and the measurement is $Q_{StarSensor}$. According to r_{GPS} , v_{GPS} , and $Q_{StarSensor}$, the Euler angles $\varphi_m, \theta_m, \psi_m$ can be calculated.

The measurement equations for the gyro measuring angular velocity are

$$\begin{cases} \omega_{Gyro} = \omega_{real} + \mu_{Gyro,\omega} + \varepsilon_{Gyro,\omega} \\ \omega_{real} = r_{install} \cdot \omega \end{cases} \quad (28)$$

where $r_{install}$ is the install vector of gyro, $\sigma_{Gyro,\omega}$ is the variance of random error, and the measured angular velocity component is $\omega_{Gyro} = [\omega_{xGyro}, \omega_{yGyro}, \omega_{zGyro}]^T$.

The state variables of the power subsystem are measured by the corresponding sensors, and the measurements follow a normal distribution:

$$\theta_{i,SunSensor} = \theta_{SW_i} + N(\mu_{sensor,\theta_{SW}}, \sigma_{sensor,\theta_{SW}}), i = 1, 2 \quad (29)$$

$$P_{Wing_{i,m}} = P_{Wing_i} + N(\mu_{sensor,P_{wing}}, \sigma_{sensor,P_{wing}}), i = 1, 2 \quad (30)$$

$$U_{Wing_{i,m}} = U_{Wing_i} + N(\mu_{sensor,U_{wing}}, \sigma_{sensor,U_{wing}}), i = 1, 2 \quad (31)$$

$$I_{Wing_{i,m}} = I_{Wing_i} + N(\mu_{sensor,I_{wing}}, \sigma_{sensor,I_{wing}}), i = 1, 2 \quad (32)$$

$$Q_{Battery,m} = Q_{Battery} + N(\mu_{sensor,Q_{Battery}}, \sigma_{sensor,Q_{Battery}}) \quad (33)$$

$$P_{Battery,m} = P_{Battery} + N(\mu_{sensor,P_{Battery}}, \sigma_{sensor,P_{Battery}}) \quad (34)$$

$$I_{Battery,m} = I_{Battery} + N(\mu_{sensor,I_{Battery}}, \sigma_{sensor,I_{Battery}}) \quad (35)$$

$$U_{Battery,m} = U_{Battery} + N(\mu_{sensor,U_{Battery}}, \sigma_{sensor,U_{Battery}}) \quad (36)$$

where $N(\cdot)$ is normal distribution, and $\mu_{sensor}, \sigma_{sensor}$ represent the mean and variance of the noise measured by the sensors, respectively.

The measurement equation of the propulsion subsystem is

$$P_{Xe,m} = P_{Xe} + N(\mu_{sensor,P}, \sigma_{sensor,P}) \quad (37)$$

where $P_{Xe,m}$ is the pressure measurement of the xenon tank.

The thermal control subsystem uses the temperature sensor to measure the temperature of the node, and the measurement equation is

$$T_{i,m} = T_i + N(\mu_{sensor,T}, \sigma_{sensor,T}) \quad (38)$$

The data on board is transmitted to the ground through the telemetry remote control subsystem, and the transmission process is affected by the relative position of the receiving and sending terminal, performance, data compression, transmission loss, and other factors, the basic transport equation in logarithmic form is expressed as

$$P_{Receiver} = P_{Sender} + G_{Sender} + G_{Receiver} - L_{Space} - L_x \quad (39)$$

where $P_{Receiver}$ is the power of the receiver antenna, P_{Sender} is the sender power, G_{Sender} is the gain of the sender antenna, $G_{Receiver}$ is the gain of the receiver antenna, L_{Space} is the path loss, and L_x is the other loss; for a detailed calculation, see Reference [27].

In summary, y consists of

$$y = [r_{xGPS}, r_{yGPS}, r_{zGPS}, v_{xGPS}, v_{yGPS}, v_{zGPS}, \varphi_m, \theta_m, \psi_m, \omega_{xGyro}, \omega_{yGyro}, \omega_{zGyro}, \theta_{SW1, SunSensor}, \theta_{SW2, SunSensor}, P_{Wing_{1,m}}, P_{Wing_{2,m}}, U_{Wing_{1,m}}, U_{Wing_{2,m}}, I_{Wing_{1,m}}, I_{Wing_{2,m}}, Q_{Battery}, P_{Battery}, U_{Battery}, I_{Battery}, P_{Xe,m}, T_{i,m}] \quad (40)$$

3. Method

3.1. The Hierarchical Model Updating Method

The state variables and telemetry variables are selected, grouped, and sorted before being updated. The rule for determining whether variables need to be modified are as follows: (1) variables that have a significant impact on the system because when their change will significantly affect the other variables; (2) variables that change obviously over time; and (3) variables that are different from those on the ground or difficult to measure accurately on the ground. As for the updating sort, the variables that play a more dominant role in the system are updated earlier, and the less influential variables are updated later. The specific group strategy for the vector electric-propulsion satellite is as follows:

- Orbit-related variables

The orbit telemetry variables refer to the position vector and velocity vector in the geocentric inertial system measured by GPS. Unless the orbit performs maneuver, orbit variables are less affected by other subsystems. On the other hand, orbit variables play a greater or even more decisive role in other variables. So the updating of orbit variables is given priority. The state variables to be updated are the initial values of orbit position r_0 and velocity v_0 . In addition, there are errors during the measurement process of GPS, so the constant errors and random errors of GPS position and velocity measurement should also be considered, that is, $\mu_{GPS,r}, \sigma_{GPS,r}, \mu_{GPS,v}, \sigma_{GPS,v}$. The telemetry variables are r_{GPS} and v_{GPS} .

- Attitude-related variables

Attitude variables also have a great impact on other parts, so they are a second priority. The attitude telemetry variables are the attitude angle calculated by the attitude determination algorithm and the angular velocity measured by the gyroscope. So besides the initial Euler angles $\varphi_0, \theta_0, \psi_0$ and the initial angular velocity being updated, the error parameters of the gyro $\mu_{Gyro,\omega}, \sigma_{Gyro,\omega}, \varepsilon_{Gyro,\omega}$ and the star sensor $\mu_{StarSensor}, \sigma_{StarSensor}$ also require correction, due to their influence. The telemetry variables selected are $\varphi_m, \theta_m, \psi_m$ and ω_{Gyro} .

- Power subsystem variables

The power subsystem includes dynamic state variables of the solar wings, and electrical state variables of the solar arrays, battery, and bus loop. The state variables are the initial angles $\theta_{wing1,0}$ and $\theta_{wing2,0}$, the photoelectric conversion efficiency of the solar array η_w , and the charging coefficient k_{Charge} and discharging coefficient $k_{Discharge}$ of the battery. Telemetry variables include the solar wings variables $P_{Wing1}, P_{Wing2}, \theta_{SW1,SunSensor}, \theta_{SW2,SunSensor}$; the battery variables $I_{Battery}, Q_{Battery}, U_{Battery}, P_{Battery}$; and the bus loop variables $Q_{Loop}, Q_{Loop}, U_{Loop}, I_{Loop}, P_{Loop}$.

- Propulsion subsystem variables

Because the variables of vector electric thruster are difficult to measure accurately on the ground, it needs to be updated on orbit. The thrust variables of the electric thruster have the greatest influence on the attitude variables and the pressure of the xenon gas, so they are put in the same group for updates; they are installation attitude variables $\varphi_{TN1}^{Install}, \theta_{TN1}^{Install}, \psi_{TN1}^{Install}$, installation variables $X_{TN1}^{Install}, Y_{TN1}^{Install}, Z_{TN1}^{Install}$, and force F_{TN1} . Triaxial attitude angle, angular velocity, and xenon cylinder pressure are selected as the telemetry parameters. The attitude variables $\varphi_m, \theta_m, \psi_m, \omega_{xGyro}, \omega_{yGyro}, \omega_{zGyro}$ and xenon gas pressure $P_{Xe,m}$ are selected as the telemetry variables.

The result of grouping and the relationship between them are shown in Figure 1.

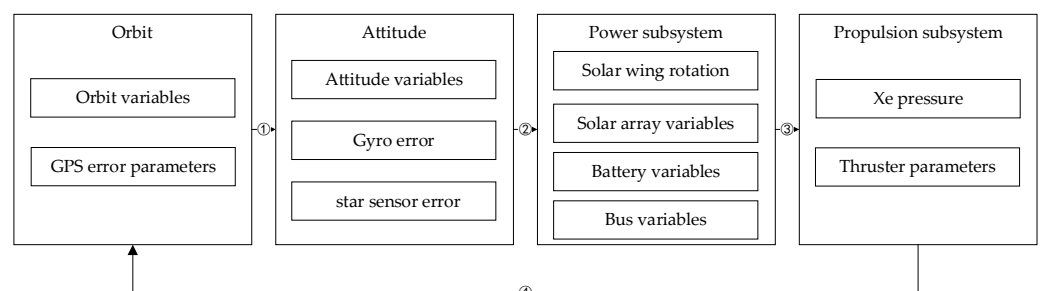


Figure 1. Hierarchical model updating diagram.

3.2. Least-Squares Method

The range of telemetry variables is determined for the normalization of telemetry data and simulation data. The initial value of the parameter x_0 to be adjusted is usually

given in a range $[x_{0,\min}, x_{0,\max}]$; a Monte Carlo method is adopted to calculate the telemetry range $[y_{\min}, y_{\max}]$ in this paper. For each x_0 , a random point is picked within its interval. All values make up a specific simulation condition. The simulation value y is obtained after running, and their minimum and maximum could be calculated. Multiple simulation conditions are generated randomly in this way. By repeating this process, after each simulation conditions run, the range of all previous simulation conditions is counted; we call it the global minimum y_{\min} and global maximum y_{\max} .

The first condition

$$y_{j,\min} = \min\{y_j(t_0), y_j(t_1), \dots, y_j(t_f)\}_1 \quad (41)$$

$$y_{j,\max} = \max\{y_j(t_0), y_j(t_1), \dots, y_j(t_f)\}_1 \quad (42)$$

For the r -th condition

$$y_{j,\min} = \min\left\{\min\{y_j(t_0), y_j(t_1), \dots, y_j(t_f)\}_{r-1}, y_{j,\min}\right\} \quad (43)$$

$$y_{j,\max} = \max\left\{\max\{y_j(t_0), y_j(t_1), \dots, y_j(t_f)\}_{r-1}, y_{j,\max}\right\} \quad (44)$$

When there are enough working conditions, y_{\min} and y_{\max} tend to be two constant values, which is the value range of y .

The least-squares method is used to update each group of variables. For the state variables and telemetry values in the k -th group as $x^{(k)}$ and $y^{(k)}$, the least-squares optimization objective is

$$\min_{x_0^{(k)}} mse(k) = \frac{1}{2} \sum_{j=1}^m \sum_{i=0}^f [\bar{y}_j^{(k),sim}(t_i) - \bar{y}_j^{(k),tele}(t_i)]^2 \quad (45)$$

where $x_0^{(k)}$ is the state value at the time t_0 , which is adjusted directly. Newton's iteration method is usually used to solve the least-squares problems for nonlinear models. The initial value $x_0^{(k,0)}$ of $x_0^{(k)}$ is given, and the simulation value is $y^{(k,0),sim}$, which becomes $\bar{y}^{(k,0),sim}$ after normalization.

Then, calculate the partial matrix of y related to x at point $x_0^{(k,0)}$, where y should be normalized as well

$$H = \begin{bmatrix} \frac{\partial \bar{y}_1}{\partial x_1} & \frac{\partial \bar{y}_1}{\partial x_2} & \dots & \frac{\partial \bar{y}_1}{\partial x_n} \\ \frac{\partial \bar{y}_2}{\partial x_1} & \frac{\partial \bar{y}_2}{\partial x_2} & \dots & \frac{\partial \bar{y}_2}{\partial x_n} \\ \vdots & \vdots & \ddots & \vdots \\ \frac{\partial \bar{y}_m}{\partial x_1} & \frac{\partial \bar{y}_m}{\partial x_2} & \dots & \frac{\partial \bar{y}_m}{\partial x_n} \end{bmatrix} \bigg|_{x_0^{(k,0)}} \quad (46)$$

For complex nonlinear models, it is common to use the difference quotient formula to displace the partial derivative, that is,

$$\frac{\partial \bar{y}_j}{\partial x_i} \approx \lim_{\Delta x_i \rightarrow 0} \frac{\bar{g}_j(x_j + \Delta x_i) - \bar{g}_j(x_i)}{\Delta x_i} \quad (47)$$

where \bar{g} means the normalized simulation value, which is the same as Equation (3).

The iteration form of x is

$$x_0^{(k,1)} = x_0^{(k,0)} + (H^T H)^{-1} H^T (\bar{y}^{(k),tele} - \bar{y}^{(k,0),sim}) \quad (48)$$

The root-mean-square error (RMSE) of telemetry variables and the relative error of state variables are calculated to evaluate the efficiency of the model updating method:

$$rmse = \sqrt{\frac{1}{mf} \sum_{j=1}^m \sum_{i=0}^f [\bar{y}_j^{sim}(t_i) - \bar{y}_j^{tele}(t_i)]^2} \quad (49)$$

$$x_{error} = \frac{|x_{est} - x_{real}|}{x_{max} - x_{min}} \times 100\% \quad (50)$$

where x_{est} is estimated value, x_{real} is real value, and x_{max} and x_{min} define the range of x .

Repeat this process until $rmse(k)$ is less than a threshold,

$$rmse(k) < \varepsilon \quad (51)$$

After the calculation of all groups is completed, the working condition of the earlier group has changed, so it is necessary to recalculate the $rmse(k)$ of each group. Furthermore, the sum of the telemetry errors of each group is calculated, and the errors $rmse_{total}$ of all the telemetry variables in the global period are calculated. Check whether $rmse_{total}$ is within the range of the threshold ε_{total} . If the accuracy is satisfied, output the result and end; otherwise, revise from Group 1 again until meets the accuracy requirement.

4. Results and Discussion

4.1. Determine the Range of Remote Measurement

Based on the initial telemetry variables value and the nominal value of the state variables, set a 10% increment as the value range of state variables; the range is shown in Table 1.

Table 1. The range of initial state variables.

Variable	Min	Max	Variable	Min	Max
r_{x0} , m	6,957,455	7,098,010	$X_{T_{N1}}^{Install}$, m	−0.45	−0.55
r_{y0} , m	60,714.48	61,941.03	$Y_{T_{N1}}^{Install}$, m	−0.9	−1.1
r_{z0} , m	529.85	540.55	$Z_{T_{N1}}^{Install}$, m	−0.8019	−0.9801
v_{x0} , m/s	−65.06	−66.37	$F_{T_{N1}}$, N	0.03969	0.04851
v_{y0} , m/s	7455.13	7605.74	$\delta_{T_{N1}}$, rad	0.015705	0.019195
v_{z0} , m/s	65.06	66.37	$\gamma_{T_{N1}}$, rad	0.0072	0.0088
$\mu_{GPS,r}$, m	−5	5	$a_{0,T_{N1}}$, m	0.09	0.11
$\sigma_{GPS,r}$, m	0	5	$a_{1,T_{N1}}$, m	0.09	0.11
$\mu_{GPS,v}$, m/s	−0.5	0.5	$d_{1,T_{N1}}$, m	−0.01	0.01
$\sigma_{GPS,v}$, m/s	0	0.5	$d_{2,T_{N1}}$, m	−0.01	0.01
φ_0 , °	−5	5	$p_{x,T_{N1}}$, m	0.09	0.11
θ_0 , °	−5	5	$p_{y,T_{N1}}$, m	0.09	0.11
ψ_0 , °	−5	5	$p_{z,T_{N1}}$, m	−0.01	0.01
ω_{x0} , °/s	−1	1	$\varphi_{T_{N1}}^{Install}$, rad	−0.75868	−0.92727
ω_{y0} , °/s	−1	1	$\theta_{T_{N1}}^{Install}$, rad	−0.1	0.1
ω_{z0} , °/s	−1	1	$\psi_{T_{N1}}^{Install}$, rad	−0.1	0.1
$\mu_{Gyro,\omega}$, °/h	−0.003	0.003	$\theta_{wing1,0}$, °	80	100
$\varepsilon_{Gyro,\omega}$, °/h	0	0.05	$\theta_{wing2,0}$, °	80	100
$\sigma_{Gyro,\omega}$, °/h	0	0.04	η_w	0.1	0.2
$\mu_{StarSensor}$, °	−0.002	0.002	k_{Charge}	0.5	1.5
$\sigma_{StarSensor}$, °	0	0.002	m_{Xe0} , kg	25	35

Take the telemetry value of position x as an example. The change in the global minimum and maximum with the condition is shown in Figure 2. It can be seen that the global minimum and global maximum gradually tend to the normal value when more

random conditions run. All telemetry variables are counted according to this process, and their feasible range is shown in Table 2.

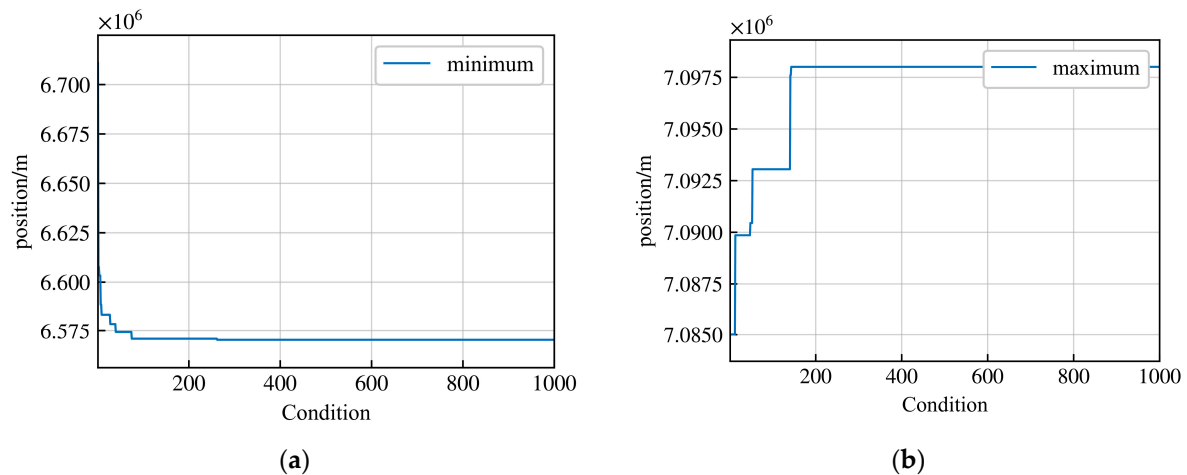


Figure 2. (a) The minimum in x position; (b) the maximum in x position.

Table 2. The feasible range of telemetry variables.

Variable	Min	Max	Variable	Min	Max
r_{xGPS} , m	6,570,369.34	7,098,007.66	Q_{Loop} , mAh	8,623,152.00	8,766,671.98
r_{yGPS} , m	60,712.16	2,301,754.64	U_{Loop} , V	28.01	83.52
r_{zGPS} , m	525.25	20,090.67	I_{Loop} , A	1.79	22.92
v_{xGPS} , m/s	−2495.26	−64.65	P_{Loop} , W	110.94	641.99
v_{yGPS} , m/s	7041.83	7606.04	$\theta_{1,SunSensor}$, °	66.28	89.97
v_{zGPS} , m/s	60.89	67.07	P_{Wing1} , W	2342.28	4873.79
φ_m , °	−21.69	21.44	$\theta_{2,SunSensor}$, °	67.31	89.99
θ_m , °	−7.05	7.21	P_{Wing2} , W	2320.98	4873.40
ψ_m , °	−22.38	21.65	$I_{Battery}$, A	20.00	20.00
ω_{xGyro} , °/s	−1.00	1.00	$Q_{Battery}$, mAh	100,005.56	101,666.67
ω_{yGyro} , °/s	−1.00	1.00	$U_{Battery}$, V	42.00	42.00
ω_{zGyro} , °/s	−1.00	1.00	$P_{Battery}$, W	840.00	840.00

4.2. The Result of Hierarchical Model Updating

The above state variables were corrected according to the updating method described in Section 3. A total of two loops of updating were carried out to compare the deviation between the state variables and the true value of each group after each updating loop, as well as the deviation of each telemetry variable RMSE.

The variation in orbit state variables is shown in Figure 3. The iteration from zero to three is the first loop of updating, and four to seven is the second loop. The state variables converge rapidly within three iterations, but the relative error is still large. After other groups were updated and the second loop was executed, the state variables could be further updated.

The updating results of orbit state variables are shown in Tables 3 and 4. Table 3 is the comparison between the state variables estimated and the true value, as well as the total residual error of telemetry variables, and Table 4 is the calculation of each telemetry variable RMSE separately.

As can be seen from Table 3, although the RMSE of telemetry variables in the first loop converges to a very small value, and most of the state variables are also updated to very small errors, the relative errors of some state variables are still large, which also indicates that the coupling effect of other variables that are not updated cannot be ignored. Through the second loop of updating, the relative errors of these state variables are further significantly reduced. The boost is one to two orders of magnitude.

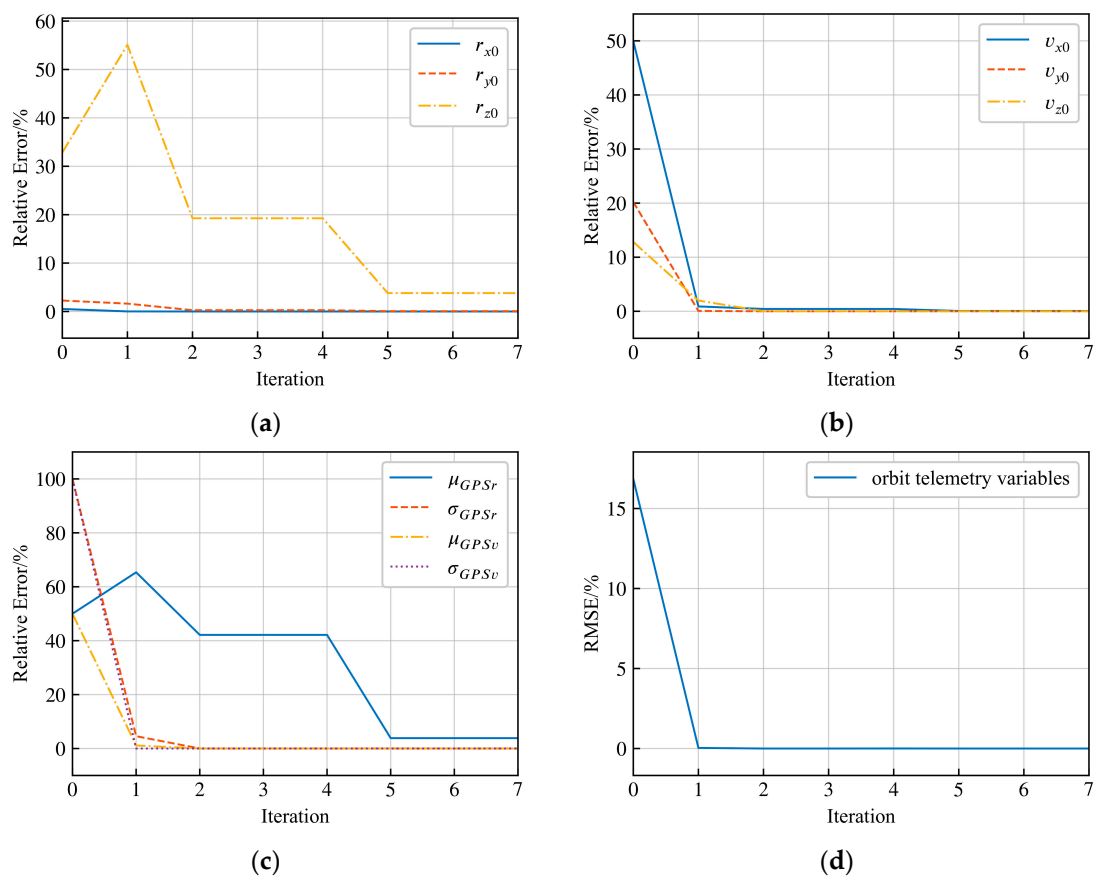


Figure 3. The variation in state variables estimation relative error and telemetry RMSE. (a) Estimation of r_0 ; (b) Estimation of v_0 ; (c) Estimation of GPS errors; (d) RMSE of orbit telemetry variables.

Table 3. The estimation of orbit state variables.

Variable	Real	The First Loop			The Second Loop		
		Estimated	Error	Relative Error	Estimated	Error	Relative Error
r_{x0} , m	7,027,732.4	7,027,728.25	4.14	0.00%	7,027,732.94	0.55	0.00%
r_{y0} , m	61,327.76	61,324.52	3.23	0.26%	61,328.61	0.86	0.07%
r_{z0} , m	535.20	531.00	4.20	39.26%	535.61	0.41	3.80%
v_{x0} , m/s	−65.72	−65.71	0.01	0.43%	−65.72	0.00	0.06%
v_{y0} , m/s	7530.43	7530.43	0.00	0.00%	7530.43	0.00	0.00%
v_{z0} , m/s	65.72	65.72	0.00	0.01%	65.72	0.00	0.01%
μ_{GPSr} , m	5.00	9.22	4.22	42.15%	4.62	0.38	3.85%
σ_{GPSr} , m	5.00	5.00	0.00	0.01%	5.00	0.00	0.02%
μ_{GPSv} , m/s	0.50	0.50	0.00	0.00%	0.50	0.00	0.00%
σ_{GPSv} , m/s	0.50	0.50	0.00	0.00%	0.50	0.00	0.00%
RMSE			0.00%			0.00%	

The same is true for each telemetry variable. After multiple loops of updating, the residual error is further reduced, and the accuracy can be improved by about one order of magnitude.

The updating results of attitude variables are shown in Tables 5 and 6. It can be seen that the state variables and telemetry variables are further improved by multiple loops of updating, and the improvement effect is one to two orders of magnitude.

Table 4. The RMSE of orbit telemetry variables.

Variable	RMSE		
	Uncorrected	The First Loop	The Second Loop
r_{xGPS}	1.11%	$2.80 \times 10^{-5}\%$	$3.6 \times 10^{-6}\%$
r_{yGPS}	0.20%	$2.42 \times 10^{-5}\%$	$8.8 \times 10^{-6}\%$
r_{zGPS}	15.12%	$9.47 \times 10^{-5}\%$	$9.03 \times 10^{-5}\%$
v_{xGPS}	1.12%	$4.46 \times 10^{-5}\%$	$9.17 \times 10^{-6}\%$
v_{yGPS}	0.53%	$3.67 \times 10^{-5}\%$	$8.03 \times 10^{-6}\%$
v_{zGPS}	38.38%	$7.7 \times 10^{-4}\%$	$7.67 \times 10^{-4}\%$

Table 5. The estimation of attitude state variables.

Variable	Real	The First Loop			The Second Loop		
		Estimated	Error	Relative Error	Estimated	Error	Relative Error
$\varphi_0, ^\circ$	1	0.94	0.06	0.64%	0.99	0.01	0.11%
$\theta_0, ^\circ$	2	2.09	0.09	0.89%	2.02	0.02	0.16%
$\psi_0, ^\circ$	3	2.90	0.10	1.00%	2.98	0.02	0.19%
$\omega_{x0}, ^\circ/s$	0.2	0.20	0.00	0.01%	0.20	0.00	0.00%
$\omega_{y0}, ^\circ/s$	0.1	0.10	0.00	0.01%	0.10	0.00	0.00%
$\omega_{z0}, ^\circ/s$	−0.1	−0.10	0.00	0.01%	−0.10	0.00	0.00%
$\mu_{Gyro,\omega}, ^\circ/h$	0.003	0.00	0.00	1.35%	0.00	0.00	0.14%
$\varepsilon_{Gyro,\omega}, ^\circ/h$	0.05	0.28	0.23	452.54%	0.08	0.03	56.27%
$\sigma_{Gyro,\omega}, ^\circ/h$	0.04	0.07	0.03	73.58%	0.05	0.01	27.73%
$\mu_{StarSensor}, ^\circ$	0.002	0.09	0.08	2083.63%	0.02	0.02	380.04%
$\sigma_{StarSensor}, ^\circ$	0.002	0.00	0.00	9.79%	0.00	0.00	0.50%
RMSE		0.09366%			0.020678%		

Table 6. The RMSE of attitude telemetry variables.

Variable	RMSE		
	Uncorrected	The First Loop	The Second Loop
φ_m	15.372%	0.109%	0.0278%
θ_m	9.215%	0.132%	0.0543%
ψ_m	13.216%	0.0874%	0.0573%
ω_{xGyro}	12.027%	0.0529%	0.00999%
ω_{yGyro}	5.157%	0.0548%	0.0102%
ω_{zGyro}	15.192%	0.0594%	0.0272%

Tables 7 and 8 show the updating result of power variables. Some errors of state variables become a little bit larger, and some become smaller, but the total RMSE of telemetry variables is further decreased.

Table 7. The estimation of power state variables.

Variable	Real	The First Loop			The Second Loop		
		Estimated	Error	Relative Error	Estimated	Error	Relative Error
$\theta_{wing1,0}, ^\circ$	90	89.14	0.86	4.29%	89.07	0.93	4.64%
$\theta_{wing2,0}, ^\circ$	90	89.14	0.86	4.29%	89.07	0.93	4.64%
η_w	0.15	0.15	0.00	0.00%	0.15	0.00	0.00%
k_{Charge}	1	1.00	0.00	0.05%	1.00	0.00	0.02%
RMSE		0.121311%			0.051712%		

Table 8. The RMSE of power telemetry variables.

Variable	RMSE		
	Uncorrected	The First Loop	The Second Loop
Q_{Loop}	11.39%	$6.46 \times 10^{-9}\%$	0.00%
U_{Loop}	24.39%	0.05%	0.02%
I_{Loop}	8.72%	0.26%	0.07%
P_{Loop}	0.28%	0.27%	0.08%
$\theta_{1,SunSensor}$	9.84%	0.09%	0.10%
P_{Wing_1}	34.27%	0.01%	0.01%
$\theta_{2,SunSensor}$	9.84%	0.09%	0.10%
P_{Wing_2}	34.27%	0.01%	0.01%
$I_{Battery}$	41.53%	$1.02 \times 10^{-8}\%$	0.00%
$Q_{Battery}$	11.39%	$6.46 \times 10^{-9}\%$	0.00%
$U_{Battery}$	0%	0%	0.00%
$P_{Battery}$	41.53%	$1.02 \times 10^{-8}\%$	0.00%

Variable modification of the propulsion subsystem is shown in Tables 9 and 10. The results of electric propulsion state variables also show that some errors decrease and some increase, but the total RMSE of telemetry variables decreases.

Table 9. The estimation of propulsion state variables.

Variable	Real	The First Loop			The Second Loop		
		Estimated	Error	Relative Error	Estimated	Error	Relative Error
$\varphi_{T_{N1}}^{Install}, \text{rad}$	−0.84298	−0.85	0.01	5.50%	−0.80	0.05	27.58%
$\theta_{T_{N1}}^{Install}, \text{rad}$	0	0.07	0.07	35.83%	−0.02	0.02	9.01%
$\psi_{T_{N1}}^{Install}, \text{rad}$	0	0.41	0.41	204.90%	0.15	0.15	73.40%
$X_{T_{N1}}^{Install}, \text{m}$	−0.5	−0.74	0.24	238.83%	−0.65	0.15	153.32%
$Y_{T_{N1}}^{Install}, \text{m}$	−1	−0.88	0.12	62.39%	−0.70	0.30	149.22%
$Z_{T_{N1}}^{Install}, \text{m}$	−0.891	−0.66	0.23	131.56%	−0.81	0.08	45.31%
$F_{T_{N1}}, \text{N}$	0.0441	0.04	0.00	0.00%	0.04	0.00	0.00%
RMSE		0.053958%			0.009247%		

Table 10. The RMSE of propulsion telemetry variables.

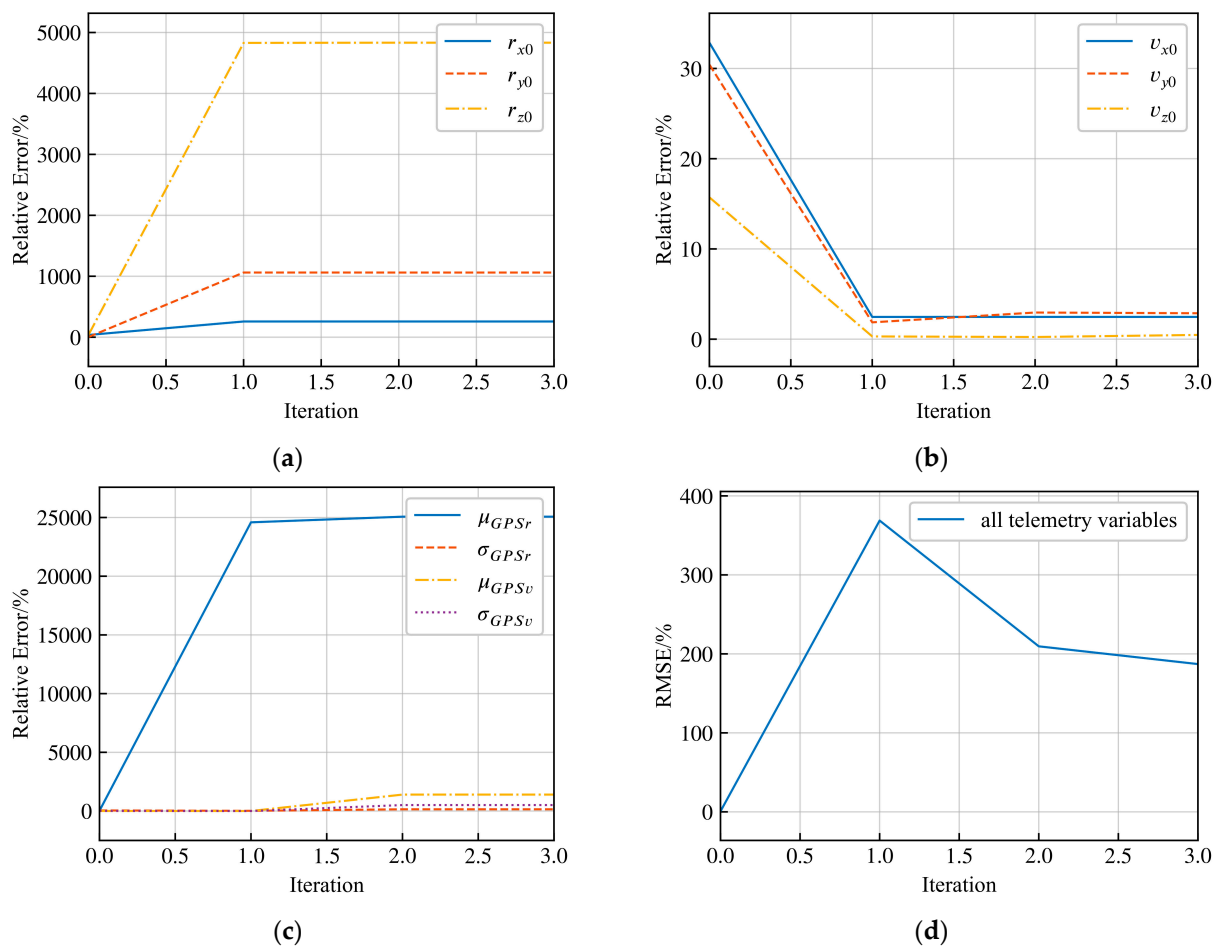
Variable	RMSE		
	Uncorrected	The First Loop	The Second Loop
φ_m	0.0988%	0.0522%	0.0237%
θ_m	0.0705%	0.0665%	0.0564%
ψ_m	0.0944%	0.0807%	0.0548%
ω_{xGyro}	0.0661%	0.0493%	0.0129%
ω_{yGyro}	0.0547%	0.0531%	0.00952%
ω_{zGyro}	0.0651%	0.0753%	0.0238%
$P_{Xe,m}$	2.686%	0%	0%

The updating result of the thruster force and moment is shown in Table 11.

To illustrate the effect of the hierarchical method, an experiment of model updating without the hierarchical method, that is, all variables were updated at the same time, was taken as a comparison. As is shown in Figure 4, most of the estimation errors grew rapidly and showed no downward trend.

Table 11. The estimation of thrust force and moment.

Variable	Real	The First Loop		The Second Loop	
		Estimated	Error	Estimated	Error
Force X in stage 1 $F_{xT_{N1}}, N$	−0.0003164	−0.0030089	0.0026925	−0.0009050	0.0005887
Force Y in stage 1 $F_{yT_{N1}}, N$	0.0051050	0.0034721	0.0016329	0.0062679	0.0011629
Force Z in stage 1 $F_{zT_{N1}}, N$	−0.0438024	−0.0438600	0.0000576	−0.0435619	0.0002405
Moment X in stage 1 $M_{xT_{N1}}, Nm$	0.0546021	0.0475862	0.0070159	0.0472978	0.0073043
Moment Y in stage 1 $M_{yT_{N1}}, Nm$	−0.0211241	−0.0283029	0.0071788	−0.0269889	0.0058648
Moment Z in stage 1 $M_{zT_{N1}}, Nm$	−0.0028563	−0.0055050	0.0026488	−0.0043405	0.0014843
Force X in stage 2 $F_{xT_{N1}}, N$	0.0022124	0.0006701	0.0015423	0.0030239	0.0008114
Force Y in stage 2 $F_{yT_{N1}}, N$	0.0013324	0.0008649	0.0004675	0.0026075	0.0012751
Force Z in stage 2 $F_{zT_{N1}}, N$	−0.0440243	−0.0440864	0.0000621	−0.0438481	0.0001763
Moment X in stage 2 $M_{xT_{N1}}, Nm$	0.0510070	0.0456808	0.0053263	0.0434219	0.0075851
Moment Y in stage 2 $M_{yT_{N1}}, Nm$	−0.0237159	−0.0311270	0.0074110	−0.0288623	0.0051464
Moment Z in stage 2 $M_{zT_{N1}}, Nm$	0.0018456	0.0000837	0.0017619	0.0003308	0.0015148

**Figure 4.** The variation in state variables estimation relative error and telemetry RMSE without the hierarchical method. (a) Estimation of r_0 ; (b) Estimation of v_0 ; (c) Estimation of GPS errors; (d) RMSE of all telemetry variables.

From the simulation result of hierarchical model updating, the RMSE of telemetry variables is significantly reduced by multi-loops iterative updating, which validates the model updating method. For the state variables, the updating results of the second loop are closer to the true values than that of the first loop.

5. Conclusions

To reflect the coupling effect between the subsystems and improve the prediction accuracy of the vector electric-propulsion satellite model, the mathematical model is established according to the whole satellite, subsystems, and devices. The state variables and telemetry variables that have a major influence are selected, grouped, and sorted by the hierarchical rules proposed. Each group is then updated by leveraging the least-squares method in sequence. The iteration loop is executed until the telemetry errors converge to the expected threshold.

The simulation results show that the residual errors of telemetry variables become smaller, and the estimation values of state variables become closer to the true value by hierarchical model updating with the close-loop iterations, which verifies the effectiveness of the hierarchical rule in solving the model updating problem of the vector electric-propulsion satellite.

The research in this paper provides a method to decompose a complex system into simple parts and solve them separately, which can not only be used for model updating of vector electric-propulsion satellites but also can be extended to other complex satellite digital twin models.

Author Contributions: Conceptualization, Y.D. and X.W.; methodology, X.W.; software, X.W.; validation, X.W.; formal analysis, X.W.; investigation, X.W.; resources, X.W.; data curation, X.W.; writing—original draft preparation, X.W.; writing—review and editing, X.W.; visualization, X.W.; supervision, Y.D.; project administration, X.W.; funding acquisition, Y.D. All authors have read and agreed to the published version of the manuscript.

Funding: This research received no external funding.

Institutional Review Board Statement: Not applicable.

Informed Consent Statement: Not applicable.

Data Availability Statement: Not applicable.

Acknowledgments: This work was partially supported by the Key Laboratory of Spacecraft Design Optimization and Dynamic Simulation Technologies, Ministry of Education.

Conflicts of Interest: The authors declare no conflict of interest.

References

1. Mazouffre, S. Electric Propulsion for Satellites and Spacecraft: Established Technologies and Novel Approaches. *Plasma Sources Sci. Technol.* **2016**, *25*, 033002. [\[CrossRef\]](#)
2. Potrivitu, G.-C.; Sun, Y.; bin Rohaizat, M.W.A.; Cherkun, O.; Xu, L.; Huang, S.; Xu, S. A Review of Low-Power Electric Propulsion Research at the Space Propulsion Centre Singapore. *Aerospace* **2020**, *7*, 67. [\[CrossRef\]](#)
3. Lev, D.; Myers, R.M.; Lemmer, K.M.; Kolbeck, J.; Koizumi, H.; Polzin, K. The Technological and Commercial Expansion of Electric Propulsion. *Acta Astronaut.* **2019**, *159*, 213–227. [\[CrossRef\]](#)
4. Wang, B.; Tao, F.; Fang, X.; Liu, C.; Liu, Y.; Freiheit, T. Smart Manufacturing and Intelligent Manufacturing: A Comparative Review. *Engineering* **2021**, *7*, 738–757. [\[CrossRef\]](#)
5. Li, L.; Lei, B.; Mao, C. Digital Twin in Smart Manufacturing. *J. Ind. Inf. Integr.* **2022**, *26*, 100289. [\[CrossRef\]](#)
6. Shafto, M.; Conroy, M.; Doyle, R.; Glaessgen, E.; Kemp, C.; LeMoigne, J.; Wang, L. *DRAFT Modelling, Simulation, Information Technology & Processing Roadmap—Technology Area 11*; National Aeronautics and Space Administration: Washington, DC, USA, 2010.
7. Kiureghian, A.D.; Ditlevsen, O. Aleatory or Epistemic? Does It Matter? *Struct. Saf.* **2009**, *31*, 105–112. [\[CrossRef\]](#)
8. Liu, X.; Li, H.; Tang, J.; Ding, Y.; Wei, L.; Yu, D.; Hu, Y. Method for Calculating Thrust Vector Eccentricity Angle of Electric Thruster. *AIAA J.* **2022**, *60*, 5060–5069. [\[CrossRef\]](#)
9. Thelen, A.; Zhang, X.; Fink, O.; Lu, Y.; Ghosh, S.; Youn, B.D.; Todd, M.D.; Mahadevan, S.; Hu, C.; Hu, Z. A Comprehensive Review of Digital Twin—Part 2: Roles of Uncertainty Quantification and Optimization, a Battery Digital Twin, and Perspectives. *Struct. Multidiscip. Optim.* **2023**, *66*, 1–43. [\[CrossRef\]](#)
10. Wang, J.; Chen, H.; Ma, J.; Zhang, T. Research on Application Method of Uncertainty Quantification Technology in Equipment Test Identification. *MATEC Web Conf.* **2021**, *336*, 02026. [\[CrossRef\]](#)
11. Levchenko, I.; Baranov, O.; Pedrini, D.; Riccardi, C.; Roman, H.E.; Xu, S.; Lev, D.; Bazaka, K. Diversity of Physical Processes: Challenges and Opportunities for Space Electric Propulsion. *Appl. Sci.* **2022**, *12*, 11143. [\[CrossRef\]](#)

12. Kokkolaras, M.; Mourelatos, Z.P.; Papalambros, P.Y. Design Optimization of Hierarchically Decomposed Multilevel Systems Under Uncertainty. *J. Mech. Des.* **2006**, *128*, 503–508. [[CrossRef](#)]
13. Oberkampf, W.L. What are validation experiments? *Exp. Tech.* **2001**, *25*, 35–40. [[CrossRef](#)]
14. Zhu, Y. Study on Model Updating and Validation Technology of Complex Mechanical Structure Based on Hierarchical Method. Ph.D. Thesis, Nanjing University of Aeronautics and Astronautics, Nanjing, China, 2010.
15. Cheng, W.; Liu, N.; Zhong, Q.; Fan, Q. Study on Parameters Correction Method of Steady-State Thermal Model for Spacecraft. *J. Astronaut.* **2010**, *31*, 270–275.
16. He, H.; Chen, Z.; He, C.; Ni, L.; Chen, G. A Hierarchical Updating Method for Finite Element Model of Airbag Buffer System under Landing Impact. *Chin. J. Aeronaut.* **2015**, *28*, 1629–1639. [[CrossRef](#)]
17. He, C.; Chen, G.; He, H.; Sun, R. Model Updating of a Dynamic System in a High-Temperature Environment Based on a Hierarchical Method. *Finite Elem. Anal. Des.* **2013**, *77*, 59–68. [[CrossRef](#)]
18. He, C.; Li, Z.; He, H.; Wang, J. Stochastic Dynamic Model Updating of Aerospace Thermal Structure with a Hierarchical Framework. *Mech. Syst. Signal Process.* **2021**, *160*, 107892. [[CrossRef](#)]
19. Chen, Z.; Zhao, Q. A Dynamic Model Updating Method with Thermal Effects Based on Improved Support Vector Regression. *Appl. Sci.* **2021**, *11*, 8025. [[CrossRef](#)]
20. Fei, C.; Liu, H.; Patricia Liem, R.; Choy, Y.; Han, L. Hierarchical Model Updating Strategy of Complex Assembled Structures with Uncorrelated Dynamic Modes. *Chin. J. Aeronaut.* **2022**, *35*, 281–296. [[CrossRef](#)]
21. Xu, J.; Xu, L.; Ma, Q.; Han, Q. Force Evaluation of Internal Cable of Prestressed Grids Based on Field Monitoring and Hierarchical Objective Model Updating. *J. Civ. Struct. Health Monit.* **2023**, *13*, 709–727. [[CrossRef](#)]
22. Li, L.; Liu, W.; Zhao, S. Study on Space Test of Electric Propulsion System. *Spacecr. Eng.* **2014**, *23*, 126–132.
23. Dong, Y.; Chen, S.; Su, J.; Hu, D. *Dynamic Simulation Technology of Satellite Attitude Control*; Science Press: Beijing, China, 2010.
24. Ren, M. Key Technologies of Autonomous Operation of Remote Sensing Satellite. Ph.D. Thesis, Beihang University, Beijing, China, 2020.
25. Li, Z. *Satellite Thermal Control Technology*; China Astronautic Publishing House: Beijing, China, 1991.
26. Craig, J.J. *Introduction to Robotics: Mechanics and Control*, 3rd ed.; Pearson Prentice Hall: Upper Saddle River, NJ, USA, 2005.
27. Xu, F. *Satellite Engineering*; China Astronautic Publishing House: Beijing, China, 2003.

Disclaimer/Publisher’s Note: The statements, opinions and data contained in all publications are solely those of the individual author(s) and contributor(s) and not of MDPI and/or the editor(s). MDPI and/or the editor(s) disclaim responsibility for any injury to people or property resulting from any ideas, methods, instructions or products referred to in the content.